A Novel Homeostatic Mechanism Tunes PI(4,5)P_2-dependent Signaling at the Plasma Membrane

Authors: Rachel C. Wills[1], Colleen P. Doyle[1], James P. Zewe[1], Jonathan Pacheco[1], Scott D. Hansen[2], Gerald R. V. Hammond[1*]

Affiliations:

[1]Department of Cell Biology, University of Pittsburgh School of Medicine; Pittsburgh, PA 15261, USA.

[2]Department of Chemistry and Biochemistry, University of Oregon; Eugene, OR 97403, USA.

*Corresponding author. Email: ghammond@pitt.edu.

One-Sentence Summary: The enzyme PIP4K functions as both a sensor and negative regulator of PI(4,5)P_2 synthesis by the closely related PIP5K enzymes, tuning the activity of numerous membrane functions.

Abstract: The lipid molecule phosphatidylinositol (4,5)-bisphosphate (PI(4,5)P_2) controls all aspects of plasma membrane (PM) function in animal cells, from its selective permeability to the attachment of the cytoskeleton. Although disruption of PI(4,5)P_2 is associated with a wide range of diseases, it remains unclear how cells sense and maintain PI(4,5)P_2 levels to support various cell functions. Here, we show that the PIP4K family of enzymes that synthesize PI(4,5)P_2 via a minor pathway, also function as sensors of tonic PI(4,5)P_2 levels, inactivating synthesis of the lipid via the major PIP5K-catalyzed pathway when PI(4,5)P_2 levels rise. Perturbation of this simple homeostatic mechanism reveals differential sensitivity of PI(4,5)P_2-dependent signaling to elevated PI(4,5)P_2 levels. These finding reveal that a subset of PI(4,5)P_2-driven functions may drive disease associated with disrupted PI(4,5)P_2 homeostasis.

Introduction

The lipid molecule PI(4,5)P_2 is a master regulator of animal cell plasma membranes (PMs). By recruiting or activating scores of membrane proteins, it controls transport of ions and solutes across the membrane [1,2], attaches the underlying cytoskeleton [3], regulates the traffic of proteinaceous cargo to and from the membrane [4], disseminates extracellular signals [2], and facilitates the entry, assembly and egress of bacterial and viral pathogens [2,5]. As a result, synthesis of PI(4,5)P_2 is essential for life in mammals [6,7]. Nonetheless, genetic defects occur in humans that either increase or decrease PI(4,5)P_2 levels, disrupting cellular physiology in unpredictable ways. These manifest in diseases ranging from cancer [8] to kidney disease [9] to dysentery [10]. Clearly, there is a central physiological imperative to tightly control PI(4,5)P_2 levels for harmonious PM function. A detailed homeostatic mechanism that can sense and maintain PI(4,5)P_2 levels has, however, proven elusive.

Most prior work in this area has focused on positive regulation of phosphatidylinositol 4-phosphate 5-kinases (PIP5Ks), the major enzymes responsible for PI(4,5)P_2 synthesis (**fig. 1A**). These enzymes add a phosphate to the 5-OH of their substrate, PI4P [11–13]. Such positive regulation can be mediated by the small GTPases Arf6 [12,13] and Rac [14,15] or the PI(4,5)P_2 metabolite phosphatidic acid [16]. In fact, PIP5Ks' strong and cooperative binding to their product, PI(4,5)P_2, generates powerful feed-forward regulation of the enzymes [17]. However, we reasoned that maintaining tonic PI(4,5)P_2 levels in the PM in the presence of abundant PI4P substrate [18,19] would demand negative feedback of PIP5Ks. This is especially apparent during lipid re-synthesis after phospholipase C (PLC) activation; PI(4,5)P_2 levels plateau despite the fact that levels of the precursor lipid PI4P are still rising [20–22]. Potential mechanisms of PIP5K downregulation include autophosphorylation [23], as well as inhibition by the related phosphatidylinositol 5-phosphate 4-kinases (PIP4Ks), which produce PI(4,5)P_2 from much less abundant PI5P substrate, but also inhibit PIP5K independent of catalytic activity [24]. Finally, a futile cycle has been proposed wherein PI(4,5)P_2 levels are held in check through dephosphorylation back to PI4P by inositol polyphosphate 5-phosphatase (INPP5) enzymes [25], although the specific INPP5 family member(s) able to execute this constitutive activity have not been defined.

Despite these many candidate effectors that could downregulate PI(4,5)P_2 synthesis, the identity of sensors that detect changing PI(4,5)P_2 levels and appropriately modulate these effectors are not known. Without knowledge of such a mechanism, how cells accomplish

effective PI(4,5)P_2 homeostasis and thereby maintain harmonious PM function has been a mystery. In this paper, we demonstrate that the PIP4K family of enzymes act as low affinity PI(4,5)P_2 sensors, monitoring tonic PI(4,5)P_2 levels and constraining PIP5K activity when levels of the lipid rise too high. Modulation of this homeostatic mechanism reveal unprecedented differences in the sensitivity of PI(4,5)P_2-dependent signaling to resting PI(4,5)P_2 levels.

Results

To elucidate the mechanism of negative feedback of PI(4,5)P_2 synthesis, we initially, independently, over-expressed all three isoforms of human PIP5K (A-C) or the single isoform from the budding yeast, *Saccharomyces cerevisiae* (Mss4). PI(4,5)P_2 levels were measured in live cells using a low-affinity biosensor, $Tubby_c^{R332H}$ [26]. In all cases, PIP5K over-expression substantially increased PI(4,5)P_2 levels (**fig. 1A**). Surprisingly, catalytic activity of the human enzymes, but not yeast PIP5K, was dispensable for promoting an increase in PI(4,5)P_2 levels at the PM (**fig. 1A**). Conversely, over-expression of the related PIP4K enzymes actually decreased PI(4,5)P_2 levels slightly, also independent of catalytic activity (**fig. 1B**). These findings are consistent with a previous study reporting the negative regulation of PIP5K by PIP4K[24]. We therefore reasoned that saturation of endogenous, inhibitory PIP4K molecules by PIP5K over-expression, regardless of catalytic activity, would free endogenous, active PIP5K enzyme from negative regulation (**fig. 1C**). In support of this, over-expression of all three PIP4K isoforms were able to attenuate the elevated PI(4,5)P_2 levels caused by PIP5K over-expression (**fig. 1D**).

To test real-time negative regulation of PIP5K activity by PIP4K, we triggered PM recruitment of cytosolic, FKBP-tagged PIP4K by chemically induced dimerization (CID) with a membrane targeted FRB domain, using rapamycin[27]. As shown in **fig. 1E**, all three isoforms of PIP4K induced a steady decline in PM PI(4,5)P_2 levels within minutes of PM recruitment, independent of catalytic activity. To test for inhibition of PIP5K by PIP4K more directly, we tested activity of purified PIP5K1A on PI4P-containing supported lipid bilayers (SLBs). Addition of PIP4K exhibited delayed inhibition of PIP5K activity (**fig. 1F**). Once PI(4,5)P_2 reached approximately 28,000 lipids/μm^2 (~2 mol %), PIP5K dependent lipid phosphorylation slowed down, which doubled the reaction completion time (**fig. 1F**, right). In contrast, we observed no PIP4K dependent inhibition of Mss4 (**fig. 1F**, inset). These data recapitulate the prior finding that PIP4K only inhibited purified PIP5K in the presence of bilayer-presented substrate[24]. We therefore hypothesized that inhibition of PIP5K by PIP4K requires recruitment of the latter enzyme to the PM by PI(4,5)P_2 itself.

To probe the interaction of endogenous PIP4Ks with PM PI(4,5)P_2, we used a split fluorescent protein approach[28] to add a NeonGreen2 (NG2) tag to PIP4K2C, the most abundant PIP4K in HEK293 cells[29,30]. Successful integration of the split NG2 tag was evident at both the genomic and protein levels (**fig. 2A**). As expected, endogenous NG2-PIP4K2C has a mainly cytosolic distribution when viewed in confocal, with a slight enrichment at the cell periphery (**fig. 2B**). Analysis of the ventral PM by total internal fluorescence microscopy (TIRFM) revealed individual, diffraction-limited and uniform intensity puncta that were dynamically associated with the membrane (**fig. 2B**). We compared the intensity of these puncta with a PI(4,5)P_2 biosensor tagged with single, dual or triple mNeonGreen copies expressed at single molecule levels. This revealed that the NG2-PIP4K2C puncta contained an average of 1.64 NG2 molecules, consistent with dimeric PIP4K2C complexes[31] containing either one or two NG2-tagged protein copies (**fig. 2B**).

Is the dynamic PM localization of NG2-PIP4K2C PI(4,5)P_2 dependent? This is indeed the case, as acute depletion of PI(4,5)P_2 by CID of a PI(4,5)P_2 5-OH phosphatase and a PM bait[27] caused rapid depletion of both a high affinity PI(4,5)P_2 biosensor, Tubby[26], and endogenous PIP4K2C (**fig. 2C**). A PI(4,5)P_2 phosphatase also rapidly depleted bound biosensor and purified PIP4K2A from supported lipid bilayers (**fig. 2D**). Since a relatively small fraction of PIP4K2C is present on the PM at steady state (see confocal images in **fig. 2B**), could elevated PI(4,5)P_2 actually enhance recruitment of PIP4K2C? To answer this question, we used CID to acutely recruit a homodimeric mutant PIP5K domain[32] to the PM (**fig. 2E**). This caused rapid increases in PM levels of both PI(4,5)P_2 biosensor and NG2-PIP4K2C, in a manner that was dependent on catalytic activity of the mutant PIP5K. Likewise, over-expression of active yeast Mss4 (but not its inactive mutant) increased PM recruitment of NG2-PIP4K2C (**fig. 2F**). In PI4P-containing SLBs, Mss4-induced PI(4,5)P_2 synthesis also increased PIP4K2C membrane binding in a highly cooperative manner: PIP4K2C was barely detectable below 2 mol % PI(4,5)P_2, but rose sharply thereafter (**fig. 2G**). Indeed, analysis of PIP4K2C equilibrium binding on PI(4,5)P_2-containing SLBs also revealed cooperative binding of PIP4K2C above ~2 mol % PI(4,5)P_2 (**fig. 2H**).

These data suggest that PIP4K2C binds PM PI(4,5)P_2 with relatively low affinity. To test this in live cells, we assessed the kinetics of PM binding during PI(4,5)P_2 re-synthesis after strong PLC activation. Stimulation of over-expressed PLC-coupled muscarinic M3 receptors induced rapid depletion of both NG2-PIP4K2C and PI(4,5)P_2 (measured with Tubby$_c$, **fig. 2I**, top). Subsequent induction of PI(4,5)P_2 re-synthesis with the muscarinic antagonist atropine revealed much

slower rebinding of NG2-PIP4K2C to the PM compared to the $Tubby_c$ $PI(4,5)P_2$ biosensor; PIP4K2C takes almost twice as long (**fig. 2I**, bottom). Collectively, these data demonstrate that PIP4Ks are low-affinity $PI(4,5)P_2$ effectors, poised to sense both decreases and crucially, elevations in $PI(4,5)P_2$ levels in the PM.

The inhibition of PIP5K activity by PIP4Ks (**fig. 1**), and the low-affinity $PI(4,5)P_2$ binding by PIP4K (**fig. 2**) suggest the following mechanism: when $PI(4,5)P_2$ levels rise due to PIP5K activity, PIP4K is recruited to the PM, where it can directly bind and inhibit PIP5K. Indeed, whereas PIP5K PM binding is largely unaffected by PIP4K over-expression, all three isoforms of PIP4K are strongly recruited to the PM by co-expression of PIP5Ks (**fig. 3A**), as previously observed for PIP4K2A[33]. While this is consistent with a direct interaction between PIP4Ks and PIP5Ks, another possibility exists: the PIP5K dependent increase in $PI(4,5)P_2$ (**fig. 1A**) enhances PM recruitment of PIP4K (**figs. 2E, F**). Prior pull-downs of PIP5K and PIP4K from lysates required cross-linking the proteins, which may have occurred when the enzymes were simply co-localized on the PM rather than directly interacting [24]. We therefore sought to distinguish between a direct PIP5K-PIP4K binding interaction versus $PI(4,5)P_2$-induced co-enrichment on the PM. To this end, we devised an experiment whereby a bait protein (either PIP5K or control proteins) could be acutely localized to domains of the PM. This was achieved using CID of baits with an endoplasmic reticulum (ER) tethered protein, causing recruitment of the bait protein to ER-PM contact sites (**fig. 3B**). Enrichment of endogenous NG2-PIP4K2C at ER-PM contact sites was only observed when PIP5K1A was the bait; an unrelated peptide (myristoylated and palmitoylated peptide from Lyn kinase, Lyn_{11}) or Mss4 did not enrich NG2-PIP4K2C (**fig. 3B**). The use of Mss4 ruled out an effect of enhanced $PI(4,5)P_2$ generation at contact sites, since this enzyme increases $PI(4,5)P_2$ as potently as PIP5K1A (**fig. 1A**), yet does not cause recruitment of PIP4K2C. Finally, we also demonstrate that PIP4K2C binding to $PI(4,5)P_2$-containing SLBs was greatly enhanced by addition of PIP5K to the membranes, but not by Mss4 (**fig. 3C**). Clearly, PIP4K enzymes directly interact with PIP5Ks on $PI(4,5)P_2$-containing lipid bilayers.

Synthesizing all of these observations, we propose a simple homeostatic feedback loop that maintains $PI(4,5)P_2$ levels in the PM (**fig. 4A**): when $PI(4,5)P_2$ levels increase, PIP4K is recruited to the PM in sufficient quantities to inhibit PIP5K, halting further $PI(4,5)P_2$ synthesis. If $PI(4,5)P_2$ levels fall, PIP4K is one of the first $PI(4,5)P_2$ binding proteins to be released (due to its low affinity), causing disinhibition of PIP5K and recovery of $PI(4,5)P_2$. We next sought to test how perturbations of this homeostat would affect physiological function. We could produce

graded changes in resting $PI(4,5)P_2$ levels by over-expression of various components of the homeostat: enhanced PIP5K1A expression, either catalytically active or inactive, increases $PI(4,5)P_2$; a myristoylated PIP4K2A retains PM localization even at low $PI(4,5)P_2$, causing sustained reductions in $PI(4,5)P_2$; and a PM-localized $PI(4,5)P_2$ 5-OH phosphatase causes near complete ablation of the lipid. These constructs all show the expected changes in PM $PI(4,5)P_2$ compared to a control, reported by three different $PI(4,5)P_2$ biosensors. Of these, $Tubby_c$ showed the most linear response across all changes in $PI(4,5)P_2$ levels (**fig. 4B**). We then used these graded changes in steady-state PM $PI(4,5)P_2$ to investigate the concentration requirements for the lipid.

$PI(4,5)P_2$ is the substrate for PLC, the enzyme that cleaves it into second messengers diacylglycerol and inositol (1,4,5)-trisphosphate (IP_3), triggering calcium release from ER stores (**fig. 4C**). Calcium release was indeed reduced by lower $PI(4,5)P_2$ levels, but appeared to be maximal at tonic $PI(4,5)P_2$ levels; it was unaffected by increased PM $PI(4,5)P_2$. This was true for both peak calcium release and total release from stores (assessed by measuring activity in calcium-free medium, **fig. 4C**). Influx of extracellular calcium was increased by elevated $PI(4,5)P_2$ levels (**fig. 4C**), consistent with a prior report that store-operated calcium entry is enhanced by increased PIP5K activity[13]. However, IP_3-triggered calcium release appears saturated at resting $PI(4,5)P_2$. This strongly contrasts with the effects on the other $PI(4,5)P_2$ signaling pathway, class I phosphoinositide 3-OH kinase (PI3K). Epidermal growth factor (EGF) receptor stimulation activates PI3K, which converts a small fraction of $PI(4,5)P_2$ to PIP_3 (**fig. 4D**). Using a sensitive PIP_3 biosensor, we observed PIP_3 production changing proportionately with $PI(4,5)P_2$, never reaching a saturated level (**fig. 4D**).

Discussion

The work presented herein reveals a remarkably simple homeostatic mechanism for PM $PI(4,5)P_2$ levels (**fig 4A**). Here, the PIP4K family of enzymes serve as both receptor and control center, detecting $PI(4,5)P_2$ and controlling the activity of the effector, PIP5K. PIP4K's low affinity and highly co-operative binding to $PI(4,5)P_2$ makes it an excellent sensor for tonic $PI(4,5)P_2$ levels. It is poised to sense $PI(4,5)P_2$ generated in excess of the needs of the lipids' legion effector proteins, ensuring these needs are met but not exceeded. This mechanism is also complementary to a previously identified homeostasis, whereby PI4P catabolism is inactivated in cells until sufficient $PI(4,5)P_2$ has been generated [34]. By these mechanisms, cells can

ensure adequate PI(4,5)P_2 is generated to support function for the cytoskeletal assembly, small solute and ion flux, membrane traffic and cell signaling processes controlled by PI(4,5)P_2.

That PIP4K has such a crucial function for which catalytic activity is entirely dispensable is surprising. PIP4K catalytic activity varies among isoforms by almost four orders of magnitude [35]; nevertheless, the ability of the enzymes to phosphorylate PI5P is known to be crucial for many of its other physiological functions [36,37]. However, the low affinity PM PI(4,5)P_2 binding that we describe, and its inhibition of PIP5K, explain why PIP4Ks are expressed in cells in excess of PIP5K by as much as 10:1 [29,30], given that levels of its substrate PI5P are present at only 1-3 percent of the level of PIP5K substrate, PI4P [38].

The apparently linear dependence of PI3K on available PI(4,5)P_2 that we revealed after modulating PI(4,5)P_2 homeostasis (**fig. 4**) explains enhanced PI3K signaling reported in PIP4K-null cells [24,39]. Intriguingly, PIP4Ks were reported to inhibit PI3K/Akt signaling two decades ago, but the mechanism was proposed to be through removal of its PI5P substrate, which was thought to somehow enhance accumulation of PI3K lipid products PIP_3 and PI(3,4)P_2 [40]. The key evidence that it was PI5P that caused the PI3K lipid accumulation came from the observation that it could be recapitulated by the *Shigella flexneri* effector protein IpgD, which generates some PI5P from PI(4,5)P_2; this and the analogous *Salmonella* effector SopB both activate the PI3K/Akt pathway[40–42]. However, it was recently shown that both SopB and IpgD are in fact novel phosphotransferases that directly convert PI(4,5)P_2 into the PI3K signaling lipid PI(3,4)P_2, explaining how these enzymes activate Akt [43].

In conclusion, our results reveal a simple yet elegant homeostatic mechanism that controls PM PI(4,5)P_2 levels (**fig. 4A**). Perturbation of this homeostasis reveals different sensitivities of PLC and PI3K signaling, with the latter showing enhanced activation with elevated PI(4,5)P_2. This likely explains why the PI3K, and not the PLC pathway, drives the phenotype of PIP4K-null fruit flies [39]. More broadly, such differences in the sensitivity of PI(4,5)P_2-dependent PM functions to lipid concentration may go a long way in explaining the phenotypic diversity of diseases associated with dysregulated PI(4,5)P_2 metabolism. For example, they may explain why a selective inhibitor of PI3Kα can correct aberrant kidney function associated with Lowe syndrome models [9]. Indeed, experimental manipulation of PI(4,5)P_2 homeostasis will now afford the ability to determine which of the panoply of PI(4,5)P_2-dependent PM functions are dysregulated by pathological alterations – perhaps bringing novel therapeutic targets into view.

Materials and Methods

Cell culture and lipofection

HeLa (ATCC CCL-2) and HEK293A (ThermoFisher R705-07) cells were cultured in DMEM (low glucose; Life Technologies 10567022) supplemented with 10% heat-inactivated fetal bovine serum (Life Technologies 10438-034), 100 units/ml penicillin, 100µg/ml streptomycin (Life Technologies 15140122), and 1:1,000 chemically defined lipid supplement (Life Technologies 11905031) at 37˚C with a humidified atmosphere with 5% CO_2. Cells were passaged twice per week diluting 1 in 5 after dissociation in TrpLE (Life Technologies 12604039). 293A cells with endogenous PIP4K2C alleles tagged with split NeonGreen2 (NG2) were generated similarly as described [44] using a protocol we have described[45]. In brief, Platinum Cas9 (Thermo Fisher B25640) was precomplexed with gRNA and electroporated into HEK293$^{NG2\text{-}1\text{-}10}$ cells in combination with a single-stranded HDR Template (IDT). Sequences are provided in **table 2**. The HDR template contains 70 bp homology-arms, the NG2-11 sequence, and a flexible linker in frame with PIP4K2C (ATGACCGAGCTCAACTTCAAGGAGTGGCAAAAGGCCTTTACCGATATGATGGGTGGCGGC). After recovery, FACS (University of Pittsburgh Flow Cytometry Core) was used to sort NG2-positive cells. These NG2-PIP4K2C cells were cultured under identical conditions to the HeLa and HEK293A cells.

Chemicals and reagents

Rapamycin (Thermo Fisher BP2963-1) was dissolved in DMSO at 1 mM and stored as a stock at -20˚C, it was used in cells at 1 µM. EGTA (VWR EM-4100) was dissolved in water at 0.5 M and stored at room temperature, it was used in cells at 5 mM. EGF (Corning CB-40052) was dissolved in water at 100 µg/ml and stored as a stock at -20˚C, it was used in cells at 10 ng/ml. Carbachol (Thermo Fisher AC10824-0050) was dissolved in water at 50 mM and stored as a stock at -20˚C, it was used in cells at 100 µM. Atropine (Thermo Fisher AC226680100) was dissolved in 100% ethanol at 25 mM and stored as a stock at -20˚C, it was used in cells at 5 µM.

Plasmids and cloning

The EGFP (Aequorea victoria GFP containing F64L and S65T mutations) [46], mCherry (Discoma DsRed monomeric variant)[47], mTagBFP2 (Entacmaea quadricolor protein eqFP578)[48], iRFP713 (Rhodopseudomonas palustris [Rp] bacteriophytochrome BphP2)[49] and iRFP670 (RpBphP6 iRFP702 containing V112I, K174M and I247C mutations)[50] fluorophores were used in the Clontech pEGFP-C1, -C2, and -N1 backbones as described previously[45]. Mutated constructs were generated using site-directed mutagenesis using targeted pairs of DNA oligos which were custom made and supplied by Thermo Fisher. New plasmids used in this study were generated using standard restriction-ligation or by using NEBuilder HiFi DNA Assembly (New England Biolabs E552OS). HsPIP5K1A, HsPIP5K1B, Mss4_Kina, and HsPIP4K2C were obtained as human codon optimized synthetic gBlocks (IDT). Otherwise, plasmids were obtained from the sources listed in Table 1. All constructs were sequence verified using Sanger DNA sequencing. Plasmids constructed for this study are available through Addgene.

Purification of PIP5K1A and Mss4

Gene sequences encoding human PIP5K1A and yeast Mss4 kinase domain were cloned into a FastBac1 vector to create the following vectors: His6-MBP-TEV-(Gly)5-PIP5K1A (1-546aa) and His6-MBP-TEV-(Gly)5-Mss4 (379-779aa). BACMIDs and baculovirus were generated as previously described[17]. ES-Sf9 cells were infected with baculovirus using an optimized multiplicity of infection (MOI), typically 2% vol/vol, that was empirically determined from small-scale test expression. Infected cells were typically grown for 48 hours at 27ºC in ESF 921 Serum-Free Insect Cell Culture medium (Expression Systems, Cat# 96-001-01) and then harvested by centrifugation. Insect cell pellets were then washed with 1x PBS [pH 7.2] and centrifuged (3500 rpm for 10 minutes). The final cell pellet was combined with an equal volume of buffer containing 1x PBS [pH 7.2], 10% glycerol, and 2x Sigma protease inhibitor cocktail tablet solution before transferring to the -80ºC freezer for storage. For purification, frozen cells were thawed in an ambient water bath and then resuspended in buffer containing 50 mM

Na_2HPO_4 [pH 8.0], 10 mM imidazole, 400 mM NaCl, 5% glycerol, 1 mM PMSF, 5 mM BME, 100 µg/mL DNase, and 1x Sigma protease inhibitor cocktail tablet. Cells were lysed using a glass dounce homogenizer. Lysate was then centrifuged at 35,000 rpm (140,000 x g) for 60 minutes in a Beckman Ti-45 rotor at 4ºC. High speed supernatant was combined with 6 mL of Ni-NTA Agarose (Qiagen, Cat# 30230) and stirred in a beaker for 1-2 hour(s) at 4ºC. Following batch binding, resin was collected in 50 mL tubes, centrifuged, and washed with buffer containing 50 mM Na_2HPO_4 [pH 8.0], 10 mM imidazole, 400 mM NaCl, and 5 mM BME. Ni-NTA resin with His6-MBP-(Asn)10-TEV-(Gly)5-PIP5KA bound was washed in a gravity flow column with 100 mL of 50 mM Na_2HPO_4 [pH 8.0], 30 mM imidazole, 400 mM NaCl, 5% glycerol, and 5 mM BME buffer. Protein elution was achieved by washing the resin with buffer containing 50 mM Na_2HPO_4 [pH 8.0], 500 mM imidazole, 400 mM NaCl, 5% glycerol, and 5 mM BME. Peak fractions were pooled, combined with 200 µg/mL His6-TEV(S291V) protease, and dialyzed against 4 liters of buffer containing 20 mM Tris [pH 8.0], 200 mM NaCl and 2.5 mM BME for 16-18 hours at 4ºC. The next day, dialysate was combined 1:1 volumes with 20 mM Tris [pH 8.0], 1 mM TCEP to reduce the NaCl to a final concentration of 100 mM. Precipitate was removed by centrifugation (3500 rpm for 10 minutes) and a 0.22 µm syringe filtration. Clarified dialysate was bound to a MonoS cation exchange column (GE Healthcare, Cat# 17-5168-01) equilibrated with buffer containing 20 mM Tris [pH 8.0], 100 mM NaCl, and 1 mM TCEP. Proteins were resolved over a 10-100% linear gradient (0.1-1 M NaCl, 45 CV, 45 mL total, 1 mL/min flow rate). $(Gly)_{x5}$-PIP5K1A and $(Gly)_{x5}$-Mss4 eluted from the MonoS in the presence of 375-450 mM NaCl. Peak fractions containing PIP5K1A were pooled, concentrated in a 30 kDa MWCO Vivaspin 6 centrifuge tube (GE Healthcare, Cat# 28-9323-17), and loaded onto a 24 mL Superdex 200 10/300 GL (GE Healthcare, Cat# 17-5174-01) size exclusion column equilibrated in 20 mM Tris [pH 8.0], 200 mM NaCl, 10% glycerol, 1 mM TCEP. Peak fractions were concentrated to 10-50 µM using a 30 kDa MWCO Amicon centrifuge tube (Millipore Sigma) before snap freezing with liquid nitrogen. PIP5K1A and Mss4 were stored in -80ºC as single use aliquots.

Purification of PIP4K2A

The gene encoding human PIP4K2A was cloned into a pETM derived bacterial expression vector to create the following fusion protein: His6-SUMO3-(Gly)5-PIP4K2A (1-406aa). Recombinant PIP4KA was expressed in BL21 (DE3) Star E. coli (i.e. lack endonuclease for increased mRNA stability). Using 4 liters of Terrific Broth, bacterial cultures were grown at 37ºC until OD_{600}=0.6. Cultures were then shifted to 18ºC for 1 hour to cool down. Protein expression was induced with 50 µM IPTG and bacteria expressed protein for 20 hours at 18ºC before being harvested by centrifugation. For purification, cells were lysed into buffer containing 50 mM Na_2HPO_4 [pH 8.0], 400 mM NaCl, 0.4 mM BME, 1 mM PMSF (add twice, 15 minutes intervals), DNase, and 1 mg/mL lysozyme using a microtip sonicator. Lysate was centrifuged at 16,000 rpm (35,172 x g) for 60 minutes in a Beckman JA-17 rotor chilled to 4ºC. Lysate was circulated over 5 mL HiTrap Chelating column (GE Healthcare, Cat# 17-0409-01) that had been equilibrated with 100 mM $CoCl_2$ for 1 hour, washed with MilliQ water, and followed by buffer containing 50 mM Na_2HPO_4 [pH 8.0], 400 mM NaCl, 0.4 mM BME. Recombinant PIP4K2A was eluted with a linear gradient of imidazole (0-500 mM, 8 CV, 40 mL total, 2 mL/min flow rate). Peak fractions were pooled, combined with 50 µg/mL of His6-SenP2 (SUMO protease), and dialyzed against 4 liters of buffer containing 25 mM Na_2HPO_4 [pH 8.0], 400 mM NaCl, and 0.4 mM BME for 16-18 hours at 4ºC. Following overnight cleavage of the SUMO3 tag, dialysate containing His6-SUMO3, His6-SenP2, and GGGGG-PIP4K2A was recirculated for at least 1 hour over a 5 mL HiTrap(Co^{2+}) chelating column. Flow-through containing GGGGG-PIP4K2A was then concentrated in a 30 kDa MWCO Vivaspin 6 before loading onto a Superdex 200 size exclusion column equilibrated in 20 mM HEPES [pH 7], 200 mM NaCl, 10% glycerol, 1 mM TCEP. In some cases, cation exchange chromatography was used to increase the purity of GGGGG-PIP4K2A before loading on the Superdex 200. In those cases, we equilibrated a MonoS column with 20 mM HEPES [pH 7], 100 mM NaCl, 1 mM TCEP buffer. PIP4K2A (pI = 6.9) bound to the MonoS was resolved over a 10-100% linear gradient (0.1-1 M NaCl, 30 CV, 30 mL total, 1.5 mL/min flow rate). Peak fractions collected from the Superdex 200 were concentrated in a 30 kDa MWCO Amicon centrifuge tube and snap frozen at a final concentration of 20-80 µM using liquid nitrogen.

Purification of PH-PLCδ1 domain

The coding sequence of human PH-PLCδ1 (11-140aa) was expressed in BL21 (DE3) E. coli as a His6-SUMO3-(Gly)5-PLCδ1 (11-140aa) fusion protein. Bacteria were grown at 37ºC in Terrific Broth to an OD_{600} of 0.8. Cultures were shifted to 18ºC for 1 hour, induced with 0.1 mM IPTG, and allowed to express protein for 20 hours at 18ºC before being harvested. Cells were lysed into 50 mM Na_2HPO_4 [pH 8.0], 300 mM NaCl, 0.4 mM BME, 1 mM PMSF, 100 µg/mL DNase using a microfluidizer. Lysate was then centrifuged at 16,000 rpm (35,172 x g) for 60 minutes in a Beckman JA-17 rotor chilled to 4ºC. Lysate was circulated over 5 mL HiTrap Chelating column (GE Healthcare, Cat# 17-0409-01) charged with 100 mM $CoCl_2$ for 1 hour. Bound protein was then eluted with a linear gradient of imidazole (0-500 mM, 8 CV, 40 mL total, 2 mL/min flow rate). Peak fractions were pooled, combined with SUMO protease (50 µg/mL final concentration), and dialyzed against 4 liters of buffer containing 50 mM Na_2HPO_4 [pH 8.0], 300 mM NaCl, and 0.4 mM BME for 16-18 hours at 4ºC. Dialysate containing SUMO cleaved protein was recirculated for 1 hour over a 5 mL HiTrap Chelating column. Flow-through containing $(Gly)_5$-PLCδ1 (11-140aa) was then concentrated in a 5 kDa MWCO Vivaspin 20 before being loaded on a Superdex 75 size exclusion column equilibrated in 20 mM Tris [pH 8.0], 200 mM NaCl, 10% glycerol, 1 mM TCEP. Peak fractions containing $(Gly)_5$-PLCδ1 (11-140aa) were pooled and concentrated to a maximum of 75 µM (1.2 mg/mL) before freezing in liquid nitrogen.

Purification of OCRL

The coding sequence of human 5-phosphatase OCRL (234-539aa of 901aa isoform) was expressed in BL21 (DE3) E. coli as a His6-MBP-(Asn)10-TEV-(Gly)5-OCRL fusion protein. Bacteria were grown at 37ºC in Terrific Broth to an OD600 of 0.8. Cultures were shifted to 18ºC for 1 hour, induced with 0.1 mM IPTG, and allowed to express protein for 20 hours at 18ºC before being harvested. Cells were lysed into 50 mM Na H_2PO_4 [pH 8.0], 300 mM NaCl, 0.4 mM BME, 1 mM PMSF, 100 µg/mL DNase using a microfluidizer. Lysate was then centrifuged at 16,000 rpm (35,172 x g) for 60 minutes in a Beckman JA-17 rotor chilled to 4ºC. Lysate was circulated over 5 mL HiTrap Chelating

column (GE Healthcare, Cat# 17-040901) charged with 100 mM CoCl2 for 1 hour. Bound protein was eluted with a linear gradient of imidazole (0-500 mM, 8 CV, 40 mL total, 2 mL/min flow rate). Peak fractions were pooled, combined with TEV protease (75 µg/mL final concentration), and dialyzed against 4 liters of buffer containing 50 mM Na H_2PO_4 [pH 8.0], 300 mM NaCl, and 0.4 mM BME for 16-18 hours at 4ºC. Dialysate containing TEV protease cleaved protein was recirculated for 1 hour over a 5 mL HiTrap Chelating column. Flow-through containing (Gly)5-protein was then concentrated in a 5 kDa MWCO Vivaspin 20 before being loaded on a Superdex 75 (10/300 GL) size exclusion column equilibrated in 20 mM Tris [pH 8.0], 200 mM NaCl, 10% glycerol, 1 mM TCEP. Peak fractions were pooled and concentrated before snap freezing in liquid nitrogen.

Sortase mediated peptide ligation

PIP4K2A, PIP5K1A, and PH-PLCδ1 were labeled on a N-terminal (Gly)5 motif using sortase mediated peptide ligation[17,51]. Initially, a LPETGG peptide was labeled with either Alexa488, Alexa647, or Cy5 conjugated to an amine reactive N-Hydroxysuccinimide (NHS) (e.g. NHS-Alexa488). Protein labeling was achieved by combining the fluorescently labeled LPETGG peptide with the following reagents: 50 mM Tris [pH 8.0], 150 mM NaCl, 50 µM $(Gly)_5$-protein, 500 µM Alexa488-LPETGG, and 10-15 µM His_6-Sortase. This reaction mixture was incubated at 16-18ºC for 16-20 hours, before buffer exchange with a G25 Sephadex column (e.g. PD10) to remove the majority of dye and dye-peptide. The His_6-Sortase was then captured on Ni-NTA agarose resin (Qiagen) and unbound labeled protein was separated from remaining fluorescent dye and peptide using a Superdex 75 or Superdex 200 size exclusion column (24 mL bed volume).

Preparation of small unilamellar vesicles

The following lipids were used to generated small unilamellar vesicles (SUVs): 1,2-dioleoyl-sn-glycero-3-phosphocholine (18:1 DOPC, Avanti # 850375C), L-α-phosphatidylinositol-4-phosphate (Brain PI(4)P, Avanti Cat# 840045X), L-α-phosphatidylinositol-4,5-bisphosphate (Brain PI(4,5)P_2, Avanti # 840046X), and 1,2-

dioleoyl-sn-glycero-3-phospho-L-serine (18:1 DOPS, Avanti # 840035C). Lipids were purchased as single use ampules containing between 0.1-5 mg of lipids dissolved in chloroform. Brain PI(4)P and PI(4,5)P_2 were purchased as 0.25 mg/mL stocks dissolved in chloroform:methanol:water (20:9:1). To make liposomes, 2 µmoles total lipids were combined in a 35 mL glass round bottom flask containing 2 mL of chloroform. Lipids were dried to a thin film using rotary evaporation with the glass round-bottom flask submerged in a 42ºC water bath. After evaporating all the chloroform, the round bottom flask was flushed with nitrogen gas for at least 30 minutes. We resuspended the lipid film in 2 mL of PBS [pH 7.2], making a final concentration of 1 mM total lipids. All lipid mixtures expressed as percentages (e.g. 98% DOPC, 2% PI(4)P) are equivalent to molar fractions. For example, a 1 mM lipid mixture containing 98% DOPC and 2% PI(4)P is equivalent to 0.98 mM DOPC and 0.02 mM PI(4)P. To generate 30-50 nm SUVs, 1 mM total lipid mixtures were extruded through a 0.03 µm pore size 19 mm polycarbonate membrane (Avanti #610002) with filter supports (Avanti #610014) on both sides of the PC membrane. Hydrated lipids at a concentration of 1 mM were extruded through the PC membrane 11 times.

Preparation of supported lipid bilayers

Supported lipid bilayers were formed on 25x75 mm coverglass (IBIDI, #10812). Coverglass was first cleaned with 2% Hellmanex III (Fisher, Cat#14-385-864) heated to 60-70ºC in a glass coplin jar and incubated for at least 30 minutes. We washed the coverglass extensively with MilliQ water and then etched with Pirahna solution (1:3, hydrogen peroxide:sulfuric acid) for 10-15 minutes the same day SLBs were formed. Etched coverglass, in water, was rapidly dried with nitrogen gas before adhering to a 6-well sticky-side chamber (IBIDI, Cat# 80608). SLBs were formed by flowing 30 nm SUVs diluted in PBS [pH 7.2] to a total lipid concentration of 0.25 mM. After 30 minutes, IBIDI chambers were washed with 5 mL of PBS [pH 7.2] to remove non-absorbed SUVs. Membrane defects were blocked for 15 minutes with a 1 mg/mL beta casein (Thermo FisherSci, Cat# 37528) diluted in 1x PBS [pH 7.4]. Before use as a blocking protein, frozen 10 mg/mL beta casein stocks were thawed, centrifuged for 30 minutes at 21,370 x g, and 0.22 µm syringe filtered. After blocking SLBs with beta casein,

membranes were washed again with 1mL of PBS, followed by 1 mL of kinase buffer before TIRFM.

Microscopy

For all live-cell imaging experiments, cells were imaged in 1.6 mL of experiment specific imaging media. Base imaging media contained FluoroBrite DMEM (Life Technologies A1896702) supplemented with 25 mM HEPES (pH 7.4) and 1:1000 chemically defined lipid supplement (SF CHIM). Media was then further supplemented with either 10% fetal bovine serum (CHIM) or 0.1% BSA (0.1% BSA CHIM). Alternatively, Ca^{2+} free Ringer's solution (Ca^{2+} Free) was used, containing 160 mM NaCl, 2.5 mM KCl, 1 mM $MgCl_2$, 8 mM glucose and 10 mM NaHEPES, pH 7.5. For treatments, 0.4 mL of experiment specific imaging media containing fivefold final concentration of compound was applied to the dish (or 0.5 ml for a second addition).

Confocal imaging was performed on a Nikon TiE A1R platform with acquisition in resonant mode with a 100x 1.45 NA plan-apochromatic objective. The signal-to-noise ratio was improved by taking 8 or 16 frame averages. Excitation of fluorophores was accomplished using a dual fiber-coupled LUN-V laser launch with 405-nm (BFP), 488-nm (EGFP and NG2), 561-nm (mCherry), and 640-nm (iRFP) lines. Emission was collected on four separate photomultiplier tubes with blue (425-475 nm), green (500-550 nm), yellow/orange (570-620 nm), and far-red (663-737 nm) filters. Blue and yellow/orange channels were recorded concurrently, as were green and far-red. The confocal pinhole was defined as 1.2x the Airy disc size of the longest wave-length channel used in the experiment. Nikon Elements denoising software was used to further enhance the signal-to-noise ratio.

For TIRFM and single-molecule imaging (SMol), a separate Nikon TiE platform coupled with a Nikon TIRF illuminator arm and 100x 1.45 NA plan-apochromatic objective was used. Excitation of fluorophores was accomplished using an Oxxius L4C laser launch with 405-nm (BFP), 488-nm (EGFP and NG2), 561-nm (mCherry), and 638-nm (iRFP) lines. Emission was collected through dual-pass filters (Chroma) with blue (420-480 nm) and yellow/orange (570-620 nm) together, and green (505-550 nm) and far-red (650-

850 nm) together. An ORCA-Fusion BT sCMOS camera (Hamamatsu) was used to capture images. For TIRFM, images were captured with 2x2 pixel binning. For SMol, the NG2 channel was excited with 20% power for 50 ms from the 488-nm laser in a 16x16 µm region of the PM. Images were registered in rolling shutter mode with 2x2 pixel binning with a 1.5x magnifier lens.

For all types of imaging, Nikon Elements software was used to acquire all images for all experiments and all data was saved with the ND2 file extension.

Membrane binding and lipid phosphorylation reactions reconstituted on supported lipid bilayers (SLBs) were visualized using an inverted Nikon Eclipse Ti2 microscope using a 100x Nikon (1.49 NA) oil immersion TIRF objective. TIRF microscopy images of SLBs were acquired using an iXion Life 897 EMCCD camera (Andor Technology Ltd., UK). Fluorescently labeled proteins were excited with either a 488 nm, 561 nm, or 637 nm diode laser (OBIS laser diode, Coherent Inc. Santa Clara, CA) controlled with a Vortran laser drive with acousto-optic tunable filters (AOTF) control. The power output measured through the objective for single particle imaging was 1-2 mW. Excitation light was passed through the following dichroic filter cubes before illuminating the sample: (1) ZT488/647rpc and (2) ZT561rdc (ET575LP) (Semrock). Fluorescence emission was detected on the iXion Life 897 EMCCD camera position after a Nikon emission filter wheel housing the following emission filters: ET525/50M, ET600/50M, ET700/75M (Semrock). All experiments were performed at room temperature (23ºC). Microscope hardware was controlled by Nikon NIS elements.

Image analysis

Analysis of all images was accomplished using Fiji software[52] using the LOCI BioFormats importer[53]. Custom macros were written to generate channel-specific montages displaying all x,y positions captured in an experiment in concatenated series. In these montages, individual regions of interest (ROIs) were generated around displayed cells.

For confocal images, the ratio or fluorescence intensity between specific compartments was analyzed as described previously[45]. In brief, a custom macro was used to generate a compartment of interest specific binary mask through à trous wavelet decomposition[54]. This mask was applied to measure the fluorescence intensity within the given compartment while normalizing to the mean pixel intensity in the ROI.

For TIRFM images, a minimum intensity projection was used to generate ROIs within the smallest footprint of the cells. Background fluorescence was measured and subtracted from all images at all timepoints. The average pixel intensity in each frame (F_t) was normalized to the mean pixel intensity in the ROI of the time points before treatment (F_{pre}) to yield F_t/F_{pre}.

Quantitative data was imported into Prism 8 (GraphPad) for statistical analysis and the generation of graphs and plots. D'Agostino and Pearson normality tests showed data that significantly varied from normal distribution, data were then subjected to a nonparametric Kruskal-Wallis test. If significant difference was found between sample medians, a post hoc Dunn's multiple comparison test was run.

Representative images were selected based on fluorescence measurements near the median of the sampled population, displayed typical morphology, and robust signal-to-noise ratio. If adjusting brightness or contrast, any changes were made across the entire image.

Single Molecule Analysis using Thunderstorm

Mean photon count was estimated using the Fiji ThunderSTORM plugin[55]. Either HEK293A cells expressing PH-PLCδ1-mNG2x1-3 or NG2-PIP4K2C cells were imaged using SMol settings. Raw images were run through Fiji using the ThunderSTORM plugin. Settings for molecule localization were determined using a wavelet filter with a local maximum method and integrated Gaussian point spread function. To determine fluorescence intensity per spot, histograms of photon counts, in each condition, were generated using a 5-photon bin size.

Kinetic measurements of PI(4,5)P_2 production

The kinetics of PI(4)P phosphorylation was measured on SLBs formed in IBIDI chambers and visualized using TIRF microscopy as previously described[17]. Reaction buffer contained 20 mM HEPES [pH 7.0], 150 mM NaCl, 1 mM ATP, 5 mM $MgCl_2$, 0.5 mM EGTA, 20 mM glucose, 200 µg/mL beta casein (ThermoScientific, Cat# 37528), 20 mM BME, 320 µg/mL glucose oxidase (Serva, #22780.01 Aspergillus niger), 50 µg/mL catalase (Sigma, #C40-100MG Bovine Liver), and 2 mM Trolox (UV treated, see methods below). Perishable reagents (i.e. glucose oxidase, catalase, and Trolox) were added 5-10 minutes before image acquisition. For all experiments, we monitored the change in PI(4)P or PI(4,5)P_2 membrane density using solution concentrations of 20 nM Alexa647-DrrA(544-647) or 20 nM Alexa488-PLCδ1, respectively.

Tables S1 and S2

Plasmid	Vector	Insert	Reference
EGFP	pEGFP-C1	EGFP	This study
EGFP-PIP5K1A	pEGFP-C1	EGFP:PIP5K1A	This study
EGFP-PIP5K1A^{D322K}	pEGFP-C1	EGFP:PIP5K1A(D322K)	This study
EGFP-PIP5K1B	pEGFP-C1	EGFP:PIP5K1B	This study
EGFP-PIP5K1B^{D266K}	pEGFP-C1	EGFP:PIP5K1B(D266K)	This study
EGFP-PIP5K1C	pEGFP-C2	EGFP:PIP5K1C	[56]
EGFP-PIP5K1C^{D316K}	pEGFP-C2	EGFP:PIP5K1C(D316K)	[56]
TagBFP2-Mss4-Kina	pTagBFP2-C1	mTagBFP2:*S. cerevisiae* Mss4(377-756)	This study
TagBFP2-Mss4^{D636K}-Kina	pTagBFP2-C1	mTagBFP2:*S. cerevisiae* Mss4(377-756)(D636K)	This study
TagBFP2	pTagBFP2-C1	mTagBFP2	This study
TagBFP2-PIP4K2A	pTagBFP2-C1	mTagBFP2:PIP4K2A	[57] This study
TagBFP2-PIP4K2A^{D273K}	pTagBFP2-C1	mTagBFP2:PIP4K2A(D273K)	This study
TagBFP2-PIP4K2B	pTagBFP2-C1	mTagBFP2:PIP4K2B	[57] This study
TagBFP2-PIP4K2C	pTagBFP2-C1	mTagBFP2:PIP4K2A	This study
mCherry-FKBP-PIP4K2A	pmCherry-C1	mCherry:FKBP1A(3-108):[GGSA]$_4$GG:PIP4K2A	[57] This study
mCherry-FKBP-PIP4K2A^{D273K}	pmCherry-C1	mCherry:FKBP1A(3-108):[GGSA]$_4$GG:PIP4K2A(D273K)	This study
mCherry-FKBP-PIP4K2B	pmCherry-C1	mCherry:FKBP1A(3-108):[GGSA]$_4$GG:PIP4K2B	[57] This study
mCherry-FKBP-PIP4K2C	pmCherry-C1	mCherry:FKBP1A(3-108):[GGSA]$_4$GG:PIP4K2C	This study
EGFP-INPP5E	pEGFP-C2	EGFP:*Mus musculus* INPP5E	[58]
Lyn$_{11}$-FRB-iRFP	piRFP-N1	LYN(1-11):MTOR(2021-2113):iRFP	[19]
TagBFP2-FKBP-INPP5E	pTagBFP2-C1	mCherry:FKBP1A(3-108):[GGSA]$_4$GG:INPP5E(214-644)	[19]

TagBFP2-FKBP-INPP5E^{D477N}	pTagBFP2-C1	mCherry:FKBP1A(3-108):[GGSA]$_4$GG:INPP5E(214-644)(D477N)	This study
mCherry-Mss4-Kina	pmCherry-C1	mCherry:*S. cerevisiae* Mss4 (377-756)	This study
mCherry-Mss4^{D636K}-Kina	pmCherry-C1	mCherry:*S. cerevisiae* Mss4 (377-756)(D636K)	This study
TagBFP2-FKBP-PIP5K1C_Kina-HD	pTagBFP2-C1	mTagBFP2:FKBP1A(3-108):[GGSA]$_4$GG:PIP5K1C(79-366)(D101R/R304D)	This study
TagBFP2-FKBP-PIP5K1C_Kina-HD^{D316K}	pTagBFP2-C1	mTagBFP2:FKBP1A(3-108):[GGSA]$_4$GG:PIP5K1C(79-366)(D101R/R304D/D316K)	This study
HAx3-AChR-M3	pcDNA3.1	HAx3:CHRM3(2-590)	J. Wess
TagBFP2-HRAS-CAAX	pTagBFP2-C1	TagBFP2:HRAS(172-189)	[59]
iRFP713-FRB-PIP5K1A	piRFP-C1	iRFP713:MTOR(2021-2113):GGSA$_2$:PIP5K1A	This study
iRFP713-FRB-Mss4-Kina	piRFP-C1	iRFP713:MTOR(2021-2113):GGSA$_2$:*S. cerevisiae* Mss4 (377-756)	This study
TagBFP2-FKBP-CYB5Atail	pTagBFP2-C1	mTagBFP2:FKBP1A(3-108):[GGSA]$_4$GG:CYB5A(100-134)	[45]
mCherry-FKBP-PIP4K2A-Kina	pmCherry-C1	mCherry:FKBP1A(3-108):[GGSA]$_4$GG:PIP4K2A(33-406)	This study
EGFP-INPP5E-CAAX	pEGFP-C1	EGFP:INPP5E(214-644):HRAS(172-189)	This study
Lyn$_{11}^{C3S}$-EGFP	pEGFP-N1	LYN(1-11)(C3S):EGFP	This study
EGFP-Lyn$_{11}^{C32S}$-PIP4K2A	pEGFP-C1	EGFP:LYN(1-11)(C3S):PIP4K2A	This study
Tubby$_C$-EGFP	pEGFP-N1	*Mus musculus* Tub(243-505):EGFP	[26]
Tubby$_C^{R332H}$-EGFP	pEGFP-N1	*Mus musculus* Tub(243-505)(R332H):mCherry	[26]
Tubby$_C$-mCherry	pmCherry-N1	*Mus musculus* Tub(243-505):mCherry	[26]
Tubby$_C^{R332H}$-mCherry	pmCherry-N1	*Mus musculus* Tub(243-505)(R332H):EGFP	[26]
PH-PLCδ1-EGFP	pEGFP-N1	PLCD1v2(1-170):EGFP	[60]
NES-EGFP-PH-ARNO$^{2G-I303Ex2}$	pEGFP-C1	*X. Laevis* map2k1.L(32-44):EGFP:CYTH2(252-399)(I303E):GGSGGVDM:CYTH2(252-399)(I303E)	[59]
R-GECO1.2	pcDNA3	R-GECO1(M164R/I166V/V174L/F222L/N267S/S270T/I330M/L419I)	[61]
iRFP670-PIP5K1A	iRFP670-C1	iRFP670:PIP5K1A	This study
iRFP670-PIP4K2C	iRFP670-C1	iRFP670:PIP4K2C	This study
PH-PLCδ1-mNGx1	pmNG2-N1	PLCD1v2(1-170):mNG2	This study
PH-PLCδ1-mNGx2	pmNG2-N1	PLCD1v2(1-170): mNG2:mNG2	This study
PH-PLCδ1-mNGx3	pmNG2-N1	PLCD1v2(1-170): mNG2:mNG2:mNG2	This study
His6-OCRL	pFastBac1	His6-MBP-Asn10-TEV-Gly5-OCRL(901isoform)(234-539)	[17]
His6-PIP4K2A	pETM	His6-SUMO3- Gly5-PIP4K2A(1-406)	This study
His6-Mss4	pFastBac1	His6-MBP-TEV-Gly5-Mss4(379-779)	[62]
His6-PIP5K1A	pFastBac1	His6-MBP-TEV-Gly5-PIP5K1A(1-546)	[62]
His6-PH-PLCδ1	pETM	His6-SUMO3-Gly5-PLCD1(11-140)	[17]

Table S1. Plasmids used in this study.

Gene	crRNA sequences
PIP4K2C	TAATACGACTCACTATAGGGGAGACTATGGCGTCCTCCTGTTTAAGAGCTATGCTGGAA
	HDR sequences
PIP4K2C	CCGCTTCCGGGGTCGGGCGCCTGGATAGCTGCCGGCTCCGGCTTCCACTTGGTCGGTTGCGCGGGAGACT ATGACCGAGCTCAACTTCAAGGAGTGGCAAAAGGCCTTTACCGATATGATGGGTGGCGGCATGGCGTCCTC CTCGGTCCCACCAGCCACGGTATCGGCGGCGACAGCAGGCCCCGGCCCAGGTTTCGGCT

Table S2. HDR and gRNA sequences for PIP4K2C.

References

1. Dickson EJ, Hille B. Understanding phosphoinositides: rare, dynamic, and essential membrane phospholipids. Biochem J. 2019;476: 1–23. doi:10.1042/bcj20180022

2. Hammond GRV, Burke JE. Novel roles of phosphoinositides in signaling, lipid transport, and disease. Curr Opin Cell Biol. 2020;63: 57–67. doi:10.1016/j.ceb.2019.12.007

3. Saarikangas J, Zhao H, Lappalainen P. Regulation of the Actin Cytoskeleton-Plasma Membrane Interplay by Phosphoinositides. Physiol Rev. 2010;90: 259–289. doi:10.1152/physrev.00036.2009

4. Schink KO, Tan K-W, Stenmark H. Phosphoinositides in Control of Membrane Dynamics. Annu Rev Cell Dev Bi. 2015;32: 1–29. doi:10.1146/annurev-cellbio-111315-125349

5. Phan TK, Bindra GK, Williams SA, Poon IKH, Hulett MD. Combating Human Pathogens and Cancer by Targeting Phosphoinositides and Their Metabolism. Trends Pharmacol Sci. 2019;40: 866–882. doi:10.1016/j.tips.2019.09.006

6. Narkis G, Ofir R, Landau D, Manor E, Volokita M, Hershkowitz R, et al. Lethal Contractural Syndrome Type 3 (LCCS3) Is Caused by a Mutation in PIP5K1C, Which Encodes PIPKIγ of the Phophatidylinsitol Pathway. Am J Hum Genetics. 2007;81: 530–539. doi:10.1086/520771

7. Volpicelli-Daley LA, Lucast L, Gong L-W, Liu L, Sasaki J, Sasaki T, et al. Phosphatidylinositol-4-Phosphate 5-Kinases and Phosphatidylinositol 4,5-Bisphosphate Synthesis in the Brain*. J Biological Chem. 2010;285: 28708–28714. doi:10.1074/jbc.m110.132191

8. Semenas J, Hedblom A, Miftakhova RR, Sarwar M, Larsson R, Shcherbina L, et al. The role of PI3K/AKT-related PIP5K1α and the discovery of its selective inhibitor for treatment of advanced prostate cancer. Proc National Acad Sci. 2014;111: E3689–E3698. doi:10.1073/pnas.1405801111

9. Berquez M, Gadsby JR, Festa BP, Butler R, Jackson SP, Berno V, et al. The phosphoinositide 3-kinase inhibitor alpelisib restores actin organization and improves proximal tubule dysfunction in vitro and in a mouse model of Lowe syndrome and Dent disease. Kidney Int. 2020;98: 883–896. doi:10.1016/j.kint.2020.05.040

10. Mason D, Mallo GV, Terebiznik MR, Payrastre B, Finlay BB, Brumell JH, et al. Alteration of Epithelial Structure and Function Associated with PtdIns(4,5)P2 Degradation by a Bacterial Phosphatase. J Gen Physiology. 2007;129: 267–283. doi:10.1085/jgp.200609656

11. Jenkins GH, Fisette PL, Anderson RA. Type I phosphatidylinositol 4-phosphate 5-kinase isoforms are specifically stimulated by phosphatidic acid. J Biological Chem. 1994;269: 11547–54.

12. Honda A, Nogami M, Yokozeki T, Yamazaki M, Nakamura H, Watanabe H, et al. Phosphatidylinositol 4-Phosphate 5-Kinase α Is a Downstream Effector of the Small G Protein ARF6 in Membrane Ruffle Formation. Cell. 1999;99: 521–532. doi:10.1016/s0092-8674(00)81540-8

13. Chen Y-J, Chang C-L, Lee W-R, Liou J. RASSF4 controls SOCE and ER–PM junctions through regulation of PI(4,5)P2Regulation of SOCE and ER–PM junctions by RASSF4. J Cell Biology. 2017;216: 2011–2025. doi:10.1083/jcb.201606047

14. Halstead JR, Savaskan NE, Bout I van den, Horck FV, Hajdo-Milasinovic A, Snell M, et al. Rac controls PIP5K localisation and PtdIns(4,5)P2 synthesis, which modulates vinculin localisation and neurite dynamics. J Cell Sci. 2010;123: 3535–3546. doi:10.1242/jcs.062679

15. Chao W-T, Daquinag AC, Ashcroft F, Kunz J. Type I PIPK-α regulates directed cell migration by modulating Rac1 plasma membrane targeting and activation. J Cell Biology. 2010;190: 247–262. doi:10.1083/jcb.200911110

16. Ishihara H, Shibasaki Y, Kizuki N, Wada T, Yazaki Y, Asano T, et al. Type I Phosphatidylinositol-4-phosphate 5-Kinases CLONING OF THE THIRD ISOFORM AND DELETION/SUBSTITUTION ANALYSIS OF MEMBERS OF THIS NOVEL LIPID KINASE FAMILY*. J Biol Chem. 1998;273: 8741–8748. doi:10.1074/jbc.273.15.8741

17. Hansen SD, Huang WYC, Lee YK, Bieling P, Christensen SM, Groves JT. Stochastic geometry sensing and polarization in a lipid kinase–phosphatase competitive reaction. Proc National Acad Sci. 2019;116: 15013–15022. doi:10.1073/pnas.1901744116

18. Hammond GRV, Schiavo G, Irvine RF. Immunocytochemical techniques reveal multiple, distinct cellular pools of PtdIns4P and PtdIns(4,5)P2. Biochem J. 2009;422: 23–35. doi:10.1042/bj20090428

19. Hammond GRV, Machner MP, Balla T. A novel probe for phosphatidylinositol 4-phosphate reveals multiple pools beyond the GolgiLocalization of PtdIns4P in living cells. J Cell Biology. 2014;205: 113–126. doi:10.1083/jcb.201312072

20. Willars GB, Nahorski SR, Challiss RAJ. Differential Regulation of Muscarinic Acetylcholine Receptor-sensitive Polyphosphoinositide Pools and Consequences for Signaling in Human Neuroblastoma Cells*. J Biol Chem. 1998;273: 5037–5046. doi:10.1074/jbc.273.9.5037

21. Tóth JT, Gulyás G, Tóth DJ, Balla A, Hammond GRV, Hunyady L, et al. BRET-monitoring of the dynamic changes of inositol lipid pools in living cells reveals a PKC-dependent PtdIns4P increase upon EGF and M3 receptor activation. Biochimica Et Biophysica Acta Bba - Mol Cell Biology Lipids. 2016;1861: 177–187. doi:10.1016/j.bbalip.2015.12.005

22. Myeong J, Park C-G, Suh B-C, Hille B. Compartmentalization of phosphatidylinositol 4,5-bisphosphate metabolism into plasma membrane liquid-ordered/raft domains. Proc National Acad Sci. 2021;118: e2025343118. doi:10.1073/pnas.2025343118

23. Itoh T, Ishihara H, Shibasaki Y, Oka Y, Takenawa T. Autophosphorylation of Type I Phosphatidylinositol Phosphate Kinase Regulates Its Lipid Kinase Activity. J Biol Chem. 2000;275: 19389–19394. doi:10.1074/jbc.m000426200

24. Wang DG, Paddock MN, Lundquist MR, Sun JY, Mashadova O, Amadiume S, et al. PIP4Ks Suppress Insulin Signaling through a Catalytic-Independent Mechanism. Cell Reports. 2019;27: 1991-2001.e5. doi:10.1016/j.celrep.2019.04.070

25. Myeong J, Cruz L de la, Jung S-R, Yeon J-H, Suh B-C, Koh D-S, et al. Phosphatidylinositol 4,5-bisphosphate is regenerated by speeding of the PI 4-kinase pathway during long PLC activation. J Gen Physiol. 2020;152: e202012627. doi:10.1085/jgp.202012627

26. Quinn KV, Behe P, Tinker A. Monitoring changes in membrane phosphatidylinositol 4,5-bisphosphate in living cells using a domain from the transcription factor tubby. J Physiology. 2008;586: 2855–2871. doi:10.1113/jphysiol.2008.153791

27. Varnai P, Thyagarajan B, Rohacs T, Balla T. Rapidly inducible changes in phosphatidylinositol 4,5-bisphosphate levels influence multiple regulatory functions of the lipid in intact living cells. J Cell Biology. 2006;175: 377–382. doi:10.1083/jcb.200607116

28. Feng S, Sekine S, Pessino V, Li H, Leonetti MD, Huang B. Improved split fluorescent proteins for endogenous protein labeling. Nat Commun. 2017;8: 370. doi:10.1038/s41467-017-00494-8

29. Geiger T, Wehner A, Schaab C, Cox J, Mann M. Comparative Proteomic Analysis of Eleven Common Cell Lines Reveals Ubiquitous but Varying Expression of Most Proteins*. Mol Cell Proteomics. 2012;11: M111.014050. doi:10.1074/mcp.m111.014050

30. Cho NH, Cheveralls KC, Brunner A-D, Kim K, Michaelis AC, Raghavan P, et al. OpenCell: proteome-scale endogenous tagging enables the cartography of human cellular organization. Biorxiv. 2021; 2021.03.29.437450. doi:10.1101/2021.03.29.437450

31. Rao VD, Misra S, Boronenkov IV, Anderson RA, Hurley JH. Structure of type IIβ phosphatidylinositol phosphate kinase: A protein kinase fold flattened for interfacial phosphorylation. Cell. 1998;94: 829–839. doi:10.1016/S0092-8674(00)81741-9

32. Hu J, Yuan Q, Kang X, Qin Y, Li L, Ha Y, et al. Resolution of structure of PIP5K1A reveals molecular mechanism for its regulation by dimerization and dishevelled. Nat Commun. 2015;6: 8205. doi:10.1038/ncomms9205

33. HINCHLIFFE KA, GIUDICI ML, LETCHER AJ, IRVINE RF. Type IIα phosphatidylinositol phosphate kinase associates with the plasma membrane via interaction with type I isoforms. Biochem J. 2002;363: 563–570. doi:10.1042/bj3630563

34. Sohn M, Korzeniowski M, Zewe JP, Wills RC, Hammond GRV, Humpolickova J, et al. PI(4,5)P2 controls plasma membrane PI4P and PS levels via ORP5/8 recruitment to ER–PM contact sitesRegulation of PM PI(4,5)P2 levels via ORP5/8. J Cell Biology. 2018;217: 1797–1813. doi:10.1083/jcb.201710095

35. Clarke JH, Irvine RF. Evolutionarily conserved structural changes in phosphatidylinositol 5-phosphate 4-kinase (PI5P4K) isoforms are responsible for differences in enzyme activity and localization. Biochem J. 2013;454: 49–57. doi:10.1042/bj20130488

36. Ravi A, Palamiuc L, Loughran RM, Triscott J, Arora GK, Kumar A, et al. PI5P4Ks drive metabolic homeostasis through peroxisome-mitochondria interplay. Dev Cell. 2021;56: 1661-1676.e10. doi:10.1016/j.devcel.2021.04.019

37. Poli A, Abdul-Hamid S, Zaurito AE, Campagnoli F, Bevilacqua V, Sheth B, et al. PIP4Ks impact on PI3K, FOXP3, and UHRF1 signaling and modulate human regulatory T cell proliferation and immunosuppressive activity. Proc National Acad Sci. 2021;118: e2010053118. doi:10.1073/pnas.2010053118

38. Sarkes D, Rameh LE. A novel HPLC-based approach makes possible the spatial characterization of cellular PtdIns5P and other phosphoinositides. Biochem J. 2010;428: 375–384. doi:10.1042/bj20100129

39. Sharma S, Mathre S, Ramya V, Shinde D, Raghu P. Phosphatidylinositol 5 Phosphate 4-Kinase Regulates Plasma-Membrane PIP3 Turnover and Insulin Signaling. Cell Reports. 2019;27: 1979-1990.e7. doi:10.1016/j.celrep.2019.04.084

40. Carricaburu V, Lamia KA, Lo E, Favereaux L, Payrastre B, Cantley LC, et al. The phosphatidylinositol (PI)-5-phosphate 4-kinase type II enzyme controls insulin signaling by regulating PI-3,4,5-trisphosphate degradation. Proc National Acad Sci. 2003;100: 9867–9872. doi:10.1073/pnas.1734038100

41. Pendaries C, Tronchère H, Arbibe L, Mounier J, Gozani O, Cantley L, et al. PtdIns(5)P activates the host cell PI3-kinase/Akt pathway during Shigella flexneri infection. Embo J. 2006;25: 1024–1034. doi:10.1038/sj.emboj.7601001

42. Marcus SL, Wenk MR, Steele-Mortimer O, Finlay BB. A synaptojanin-homologous region of Salmonella typhimurium SigD is essential for inositol phosphatase activity and Akt activation. Febs Lett. 2001;494: 201–207. doi:10.1016/s0014-5793(01)02356-0

43. Walpole GFW, Pacheco J, Chauhan N, Clark J, Anderson KE, Abbas YM, et al. Kinase-independent synthesis of 3-phosphorylated phosphoinositides by a phosphotransferase. Nat Cell Biol. 2022; 1–15. doi:10.1038/s41556-022-00895-y

44. Leonetti MD, Sekine S, Kamiyama D, Weissman JS, Huang B. A scalable strategy for high-throughput GFP tagging of endogenous human proteins. Proceedings of the National Academy of Sciences. 2016;113: E3501–E3508. doi:10.1073/pnas.1606731113

45. Zewe JP, Wills RC, Sangappa S, Goulden BD, Hammond GR. SAC1 degrades its lipid substrate PtdIns4P in the endoplasmic reticulum to maintain a steep chemical gradient with donor membranes. Elife. 2018;7: e35588. doi:10.7554/elife.35588

46. Cormack BP, Valdivia RH, Falkow S. FACS-optimized mutants of the green fluorescent protein (GFP). Gene. 1996;173: 33–38. doi:10.1016/0378-1119(95)00685-0

47. Shaner NC, Campbell RE, Steinbach PA, Giepmans BNG, Palmer AE, Tsien RY. Improved monomeric red, orange and yellow fluorescent proteins derived from Discosoma sp. red fluorescent protein. Nat Biotechnol. 2004;22: 1567–1572. doi:10.1038/nbt1037

48. Subach OM, Cranfill PJ, Davidson MW, Verkhusha VV. An Enhanced Monomeric Blue Fluorescent Protein with the High Chemical Stability of the Chromophore. Plos One. 2011;6: e28674. doi:10.1371/journal.pone.0028674

49. Filonov GS, Piatkevich KD, Ting L-M, Zhang J, Kim K, Verkhusha VV. Bright and stable near infra-red fluorescent protein for in vivo imaging. Nat Biotechnol. 2011;29: 757–761. doi:10.1038/nbt.1918

50. Shcherbakova DM, Verkhusha VV. Near-infrared fluorescent proteins for multicolor in vivo imaging. Nat Methods. 2013;10: 751–754. doi:10.1038/nmeth.2521

51. Guimaraes CP, Witte MD, Theile CS, Bozkurt G, Kundrat L, Blom AEM, et al. Site-specific C-terminal and internal loop labeling of proteins using sortase-mediated reactions. Nat Protoc. 2013;8: 1787–1799. doi:10.1038/nprot.2013.101

52. Schindelin J, Arganda-Carreras I, Frise E, Kaynig V, Longair M, Pietzsch T, et al. Fiji: an open-source platform for biological-image analysis. Nat Methods. 2012;9: 676–682. doi:10.1038/nmeth.2019

53. Linkert M, Rueden CT, Allan C, Burel J-M, Moore W, Patterson A, et al. Metadata matters: access to image data in the real world. J Cell Biology. 2010;189: 777–782. doi:10.1083/jcb.201004104

54. Olivo-Marin J-C. Extraction of spots in biological images using multiscale products. Pattern Recogn. 2002;35: 1989–1996. doi:10.1016/s0031-3203(01)00127-3

55. Ovesný M, Křížek P, Borkovec J, Švindrych Z, Hagen GM. ThunderSTORM: a comprehensive ImageJ plug-in for PALM and STORM data analysis and super-resolution imaging. Bioinformatics. 2014;30: 2389–2390. doi:10.1093/bioinformatics/btu202

56. Paolo GD, Pellegrini L, Letinic K, Cestra G, Zoncu R, Voronov S, et al. Recruitment and regulation of phosphatidylinositol phosphate kinase type 1γ by the FERM domain of talin. Nature. 2002;420: 85–89. doi:10.1038/nature01147

57. Lundquist MR, Goncalves MD, Loughran RM, Possik E, Vijayaraghavan T, Yang A, et al. Phosphatidylinositol-5-Phosphate 4-Kinases Regulate Cellular Lipid Metabolism By Facilitating Autophagy. Mol Cell. 2018;70: 531-544.e9. doi:10.1016/j.molcel.2018.03.037

58. Roberts HF, Clarke JH, Letcher AJ, Irvine RF, Hinchliffe KA. Effects of lipid kinase expression and cellular stimuli on phosphatidylinositol 5-phosphate levels in mammalian cell lines. Febs Lett. 2005;579: 2868–2872. doi:10.1016/j.febslet.2005.04.027

59. Goulden BD, Pacheco J, Dull A, Zewe JP, Deiters A, Hammond GRV. A high-avidity biosensor reveals plasma membrane PI(3,4)P2 is predominantly a class I PI3K signaling product. J Cell Biology. 2019;218: 1066–1079. doi:10.1083/jcb.201809026

60. Várnai P, Balla T. Visualization of Phosphoinositides That Bind Pleckstrin Homology Domains: Calcium- and Agonist-induced Dynamic Changes and Relationship to Myo-[3H]inositol-labeled Phosphoinositide Pools. J Cell Biology. 1998;143: 501–510. doi:10.1083/jcb.143.2.501

61. Wu J, Liu L, Matsuda T, Zhao Y, Rebane A, Drobizhev M, et al. Improved Orange and Red Ca2+ Indicators and Photophysical Considerations for Optogenetic Applications. Acs Chem Neurosci. 2013;4: 963–972. doi:10.1021/cn400012b

62. Hansen SD, Lee AA, Groves JT. Membrane-mediated dimerization potentiates PIP5K lipid kinase activity. Biorxiv. 2021; 2021.09.21.461304. doi:10.1101/2021.09.21.461304

Acknowledgments: We thank Robin Irvine for critical reading of the manuscript and valuable suggestions.

Funding:

National Institutes of Health grant 2R35GM119412 (GRVH)

National Institutes of Health grant 5F31CA247349-02 (RCW)

National Science Foundation CAREER award MCB-2048060 (SDH)

Author contributions:

Conceptualization: RCW, SDH, GRVH

Investigation: RCR, JP, SDH, GRVH

Formal analysis: RCW, JP, SDH, GRVH

Resources: RCR, CPD, JPZ, JP, SDH, GRVH

Funding acquisition: RCW, GRVH

Writing – original draft: RCW, GRVH

Writing – review & editing: RCW, CPD, JPZ, JP, SDH, GRVH

Competing interests: Authors declare that they have no competing interests.

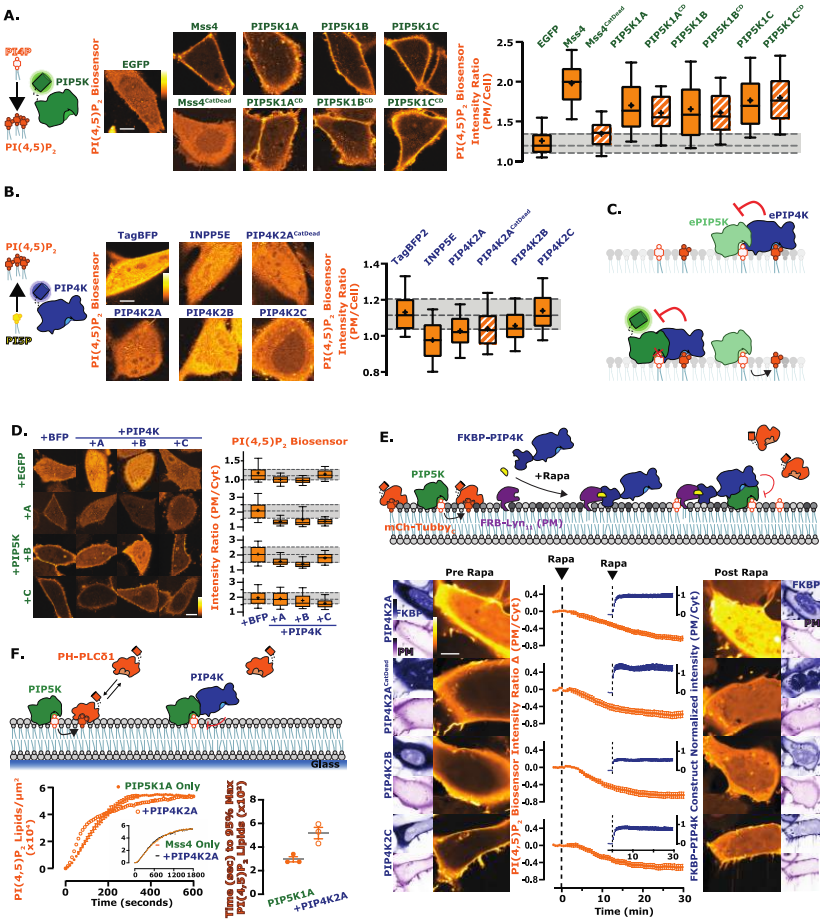

Fig. 1. Reciprocal regulation of PM PIP_2 levels by PIP5K and PIP4K. (**A**) PIP5Ks increase PM $PI(4,5)P_2$ independently of catalytic activity. Cartoon denotes the catalytic activity of PIP5K. Images show equatorial confocal sections of HeLa cells expressing the low affinity $Tubby_C^{R332H}$ $PI(4,5)P_2$ sensor (orange), co-transfected with EGFP-tagged catalytically active or dead PIP5K constructs (yeast Mss4 or mammalian A, B, or C isoforms), or EGFP alone as control. Increased $PI(4,5)P_2$ is apparent from increased $Tubby_C^{R332H}$ fluorescence in the PM. Box and whisker plots show the mean fluorescence intensity ratio (PM/cell) of the $PI(4,5)P_2$ sensor from >90 cells imaged across at least three independent experiments (boxes displaying median and interquartile range, whiskers representing 10-90% of data and "+" represents mean). (**B**) PIP4Ks decrease PM $PI(4,5)P_2$ independently of catalytic activity. Cartoon shows the catalytic activity of PIP4K. Images show $PI(4,5)P_2$ sensor in HeLa cells as in A, co-transfected with different PIP4K isoforms (A, B, C), catalytically dead PIP4K2A or a $PI(4,5)P_2$ 5-phosphatase(pptase) (INPP5E). Box and whiskers from >90 cells imaged across at least three independent experiments as in A. (**C**) Proposed inhibition of ePIP5K (endogenous PIP5K) by ePIP4K. With the overexpression of a fluorescently tagged version of PIP5K, regardless of catalytic activity, ePIP4K is sequestered. This relieves endogenous PIP5K from inhibition, increasing $PI(4,5)P_2$ levels. (**D**) PIP4Ks antagonize PIP5K-mediated $PI(4,5)P_2$ increases. HeLa cells expressing $PI(4,5)P_2$ indicator $Tubby_C^{R332H}$ (orange) were co-transfected with the indicated EGFP- or TagBFP2-tagged constructs. Images show confocal equatorial sections of representative cells. Box and whiskers from 90 cells imaged across at least three independent experiments, displayed as in A. (**E**) PIP4K recruitment acutely inhibits PM $PI(4,5)P_2$ levels. Cartoon schematics show the chemically induced dimerization (CID) system for FKBP-tagged PIP4K isoforms (A, B, C), which dimerize with the PM-anchored $FRB\text{-}Lyn_{11}$ upon the addition of rapamycin (rapa). HEK293A cells were transfected with FKBP-tagged proteins, the high affinity $PI(4,5)P_2$ indicator $Tubby_C$ and $FRB\text{-}Lyn_{11}$. During time-lapse confocal microscopy, cells were stimulated with 1 μM rapa as indicated. Graphs represent mean change in $PI(4,5)P_2$ sensor intensity ratio (PM/cell) ± s.e. for 35-60 cells imaged across three independent experiments. (**F**) PIP4K2A attenuates the kinetics of $PI(4,5)P_2$ production driven by PIP5K1A, but not Mss4. Kinetics of $PI(4,5)P_2$ production measured on SLBs in the presence of 1 nM PIP5K1A, 20 nM PH-PLCδ1, +/- 50 nM PIP4K2A. Inhibition of PIP5K1A activity is delayed until a threshold density of approximately 2% $PI(4,5)P_2$ is created to support membrane recruitment of PIP4K2A. Inset shows kinetics of reactions executed in the presence of 50 nM Mss4, 20 nM PH-PLCδ1, +/- 50 nM PIP4K2A. Initial membrane composition: 76% DOPC, 20% DOPS, 4% PI(4)P. Right graphs show the quantification of time required for reactions to reach 95% completion (n = 3 technical replicates).

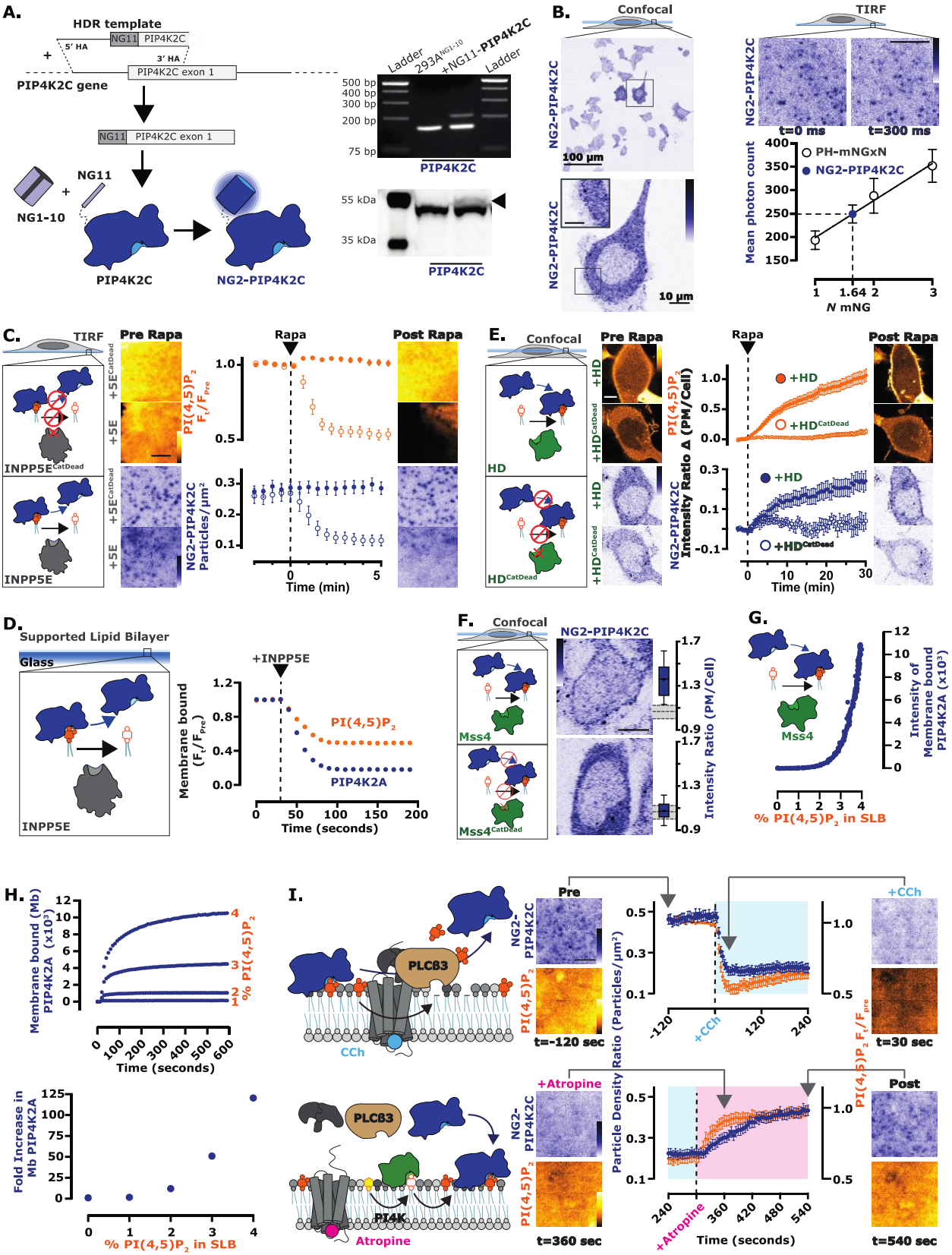

Fig. 2. PI(4,5)P_2 is necessary and sufficient for the PM localization of PIP4K. (**A**) Endogenous tagging of PIP4K2C. Brief cartoon schematic showing the mechanism of endogenous tagging employed for PIP4K2C with NeonGreen2 (NG2). The resulting cell line was termed NG2-PIP4K2C. Cells were genotyped with a mNG specific forward primer and a PIP4K2C specific reverse primer yielding an edited product of ~200bp. Cells were also probed with a PIP4K2C specific antibody showing the expected ~3 kDa shift in weight (arrowhead). (**B**) Image based characterization of NG2-PIP4K2C. Confocal images display the NG2-PIP4K2C (blue) in cells localized mainly to the cytosol, but slight association of the enzyme to the PM can be seen in the zoomed image. When imaged live by TIRF, dynamic, diffraction limited spots are observed on the membrane (compare differential localization at 0 and +0.3 s). These have an intensity consistent with a mixed population of 1 or 2 mNG molecules when calibrated against single, dimeric or trimeric mNG molecules fused to a PI(4,5)P_2 binding domain (graph). This correlates to the mean photon count of a heterogeneously tagged cell population (one or two alleles tagged with $NG2^{11}$ and dimeric PIP4K2C). (**C**) Depletion of PI(4,5)P_2 causes NG2-PIP4K2C to dissociate from the membrane. Cartoons show the CID system, in TIRF, for FKBP-tagged INPP5E (catalytically active or dead) dimerizing with the PM-anchored Lyn_{11}-FRB. NG2-PIP4K2C (blue) cells were transfected with FKBP-tagged proteins, the high affinity PI(4,5)P_2 indicator $Tubby_C$ (orange) and Lyn_{11}-FRB. During time-lapse TIRF microscopy, cells were stimulated with 1µM rapa, as indicated. $Tubby_C$ traces represent mean change in fluorescence intensity (F_t/F_{pre}) ± s.e. The NG2-PIP4K2C traces represent the mean change in puncta per μm^2 ± s.e. of 36-37 cells that were imaged across three independent experiments. (**D**) Depletion of PI(4,5)P_2 causes PIP4K2A to dissociate from SLBs. Imaging chambers containing 50 nM PIP4K2A and 20 nM PH-PLCδ1 at equilibrium with SLBs composed of 96% DOPC and 4% PI(4,5)P_2 were visualized by TIRF microscopy. At 30 seconds, 100 nM OCRL was added to catalyze the dephosphorylation of PI(4,5)P_2 and membrane dissociation of PIP4K2A and PH-PLCδ1. (**E**) Acute enrichment of PI(4,5)P_2 causes PIP4K2C to increase association with the membrane. Cartoons show the CID system, in confocal, for the interaction of catalytically active or dead FKBP-tagged homo-dimeric PIP5K1C kinase with the PM-anchored Lyn_{11}-FRB. NG2-PIP4K2C (blue) cells were transfected with FKBP-tagged proteins, the low affinity PI(4,5)P_2 indicator $Tubby_C^{R332H}$ (orange) and Lyn_{11}-FRB. During time-lapse confocal microscopy, cells were stimulated with 1µM rapa, as indicated. Traces represent mean change in fluorescence intensity (change in PM/cell ratio from pre-stimulation levels) ± s.e. of 48-52 cells imaged across at least three independent experiments. (**F**) Chronic enrichment of PI(4,5)P_2 causes NG2-PIP4K2C to associate with the membrane. Cartoons show the expression of catalytically active or dead Mss4. Images show equatorial confocal sections of representative NG2-PIP4K2C cells transfected with Mss4 and the low affinity PI(4,5)P_2 indicator $Tubby_C^{R332H}$. Box and whisker plots show the mean fluorescence intensity ratio (PM/cell) of the PI(4,5)P_2 sensor from 88-90 cells images across at least three independent experiments (boxes display median and interquartile range, whiskers represent 10-90% of data and "+" represents mean). (**G**) Enrichment of PI(4,5)P_2 causes dynamic membrane recruitment of purified PIP4K2A. In SLBs, membrane recruitment of 50 nM PIP4K2A monitored during Mss4 catalyzed phosphorylation of PI(4)P. Membranes containing 4% PI(4)P were converted to PI(4,5)P_2 using 10 nM Mss4. (**H**) Purified PIP4K2A localizes to PI(4,5)P_2 in a concentration dependent manner. Membrane absorption and equilibration kinetics of 50 nM Alexa488-PIP4K2A measured by TIRF microscopy on SLBs containing 1–4% PI(4,5)P_2. PIP4K2A membrane binding exhibited non-linearity with respect to the PI(4,5)P_2 lipid density. Quantification of the fold increase in membrane bound PIP4K2A relative to the equilibrium fluorescence intensity of PIP4K2A on a membrane containing 0% PI(4,5)P_2. (**I**) PM localization of PIP4K2C follows resynthesis of PI(4,5)P_2. Cartoons show PLCß3 mediated loss of PI(4,5)P_2 and eNG-PIP4K2C followed by the subsequent reappearance of PI(4,5)P_2 and eNG-PIP4K2C. eNG-PIP4K2C (blue) cells were transfected with FKBP-tagged proteins, the high affinity PI(4,5)P_2 indicator $Tubby_C$ (orange) and Lyn_{11}-FRB. During time-lapse TIRF microscopy, cells were stimulated with 100 µM carbachol (CCh) and then stimulated with 5 µM atropine as indicated. $Tubby_C$ traces represent mean change in fluorescence intensity (F_t/F_{pre}) ± s.e. The eNG-PIP4K traces represent the mean change in puncta per μm^2 ± s.e. 40 cells were imaged across at least three independent experiments.

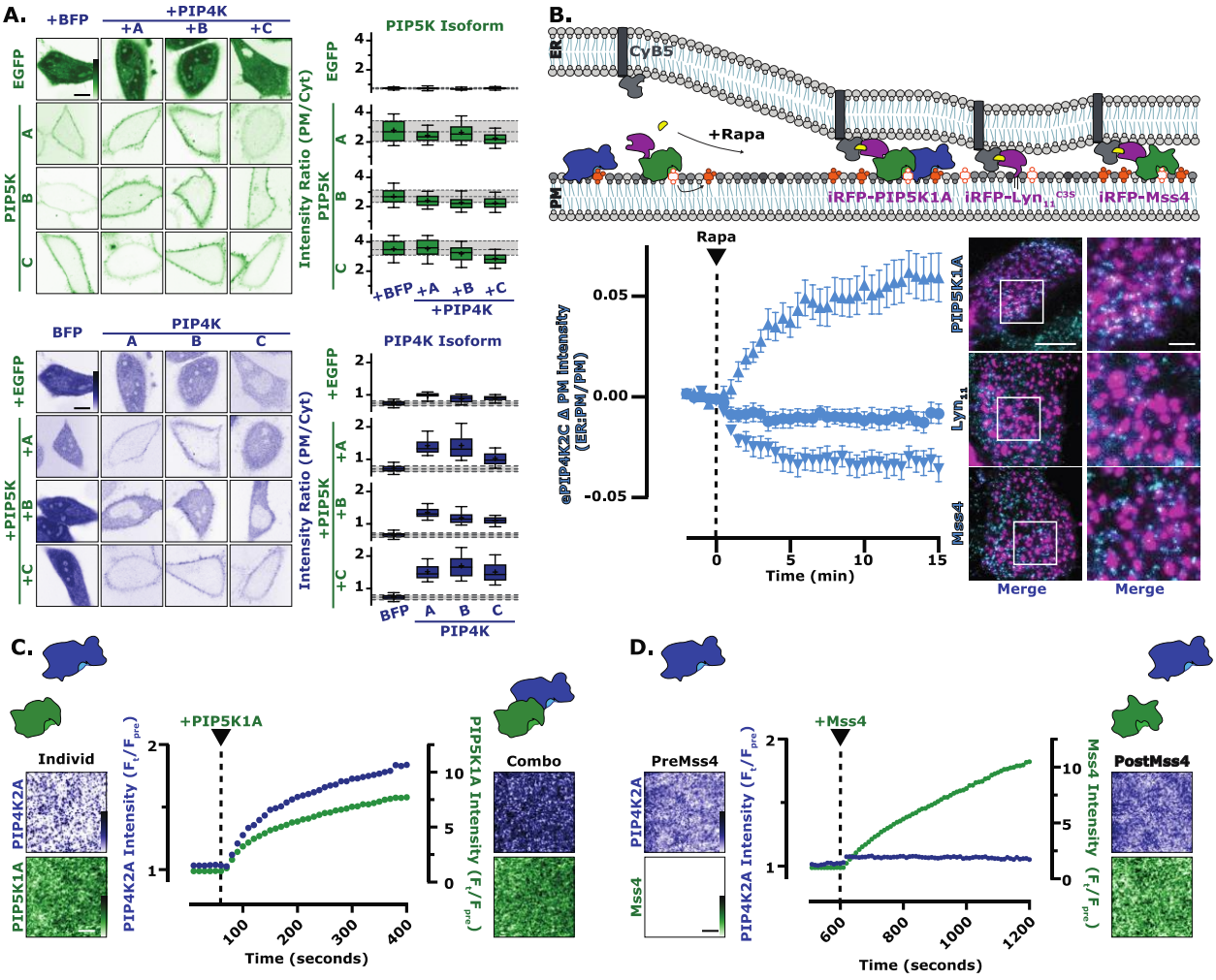

Fig. 3. PIP4K interacts with mammalian PIP5K for inhibition. (**A**) PIP5K expression increases PIP4K PM localization. The same experimental data set from Figure 1E is used here. HeLa cells expressing PIP5K (green) or PIP4K (blue) were co-transfected with the indicated EGFP- or TagBFP2-tagged isoform constructs. Images show equatorial sections in confocal of representative cells. For box and whisker plots, boxes display median and interquartile range and whiskers representing 10-90% of the data and "+" represents the mean of 90 cells imaged across at least three independent experiments. (**B**) PIP4K2C interacts with PIP5K1A. Cartoon schematic show the CID system for the generation of ER-PM contact sites between ER-anchored FKBP-CyB5 and PM-anchored FRB-tagged constructs. eNG-PIP4K2C (cyan) cells were transfected with FKBP-CyB5, the low affinity $PI(4,5)P_2$ indicator $Tubby_C^{R332H}$, and the indicated FRB-tagged construct (magenta). During time-lapse TIRF microscopy, cells were stimulated with 1μM rapa. TIRF images are representative and color-coded to represent fluorescence intensity, as indicated. eNG-PIP4K2C traces represent mean fluorescence intensities (ER:PM/PM) ± s.e. of 32-39 cells imaged across a minimum of three independent experiments. (**C**) Dynamic PIP5K1A dependent membrane recruitment of PIP4K2A. In the absence of PIP5K, 50 nM PIP4K2A displays a low level of membrane recruitment. The addition of 10 nM PIP5K1A, stimulates an immediate and steady increase in both PIP4K2A and PIP5K1A membrane localization. Membrane composition: 2% $PI(4,5)P_2$, 98% DOPC. TIRF images are representative and color-coded to represent fluorescence intensity, as indicated, scale bar is 5 μm. (**D**) Membrane binding of PIP4K2A is insensitive to yeast Mss4 membrane localization. TIRF microscopy images show the membrane localization of PIP4K2A in the absence and presence of Mss4. Following membrane equilibration of 50 nM PIP4K2A, 10 nM Mss4 was added to the imaging chamber. No appreciable change in PIP4K2A localization was observed during membrane absorption of Mss4. Membrane composition: 4% $PI(4,5)P_2$ and 96% DOPC. TIRF images are representative and color-coded to represent fluorescence intensity, as indicated, scale bar is 5 μm.

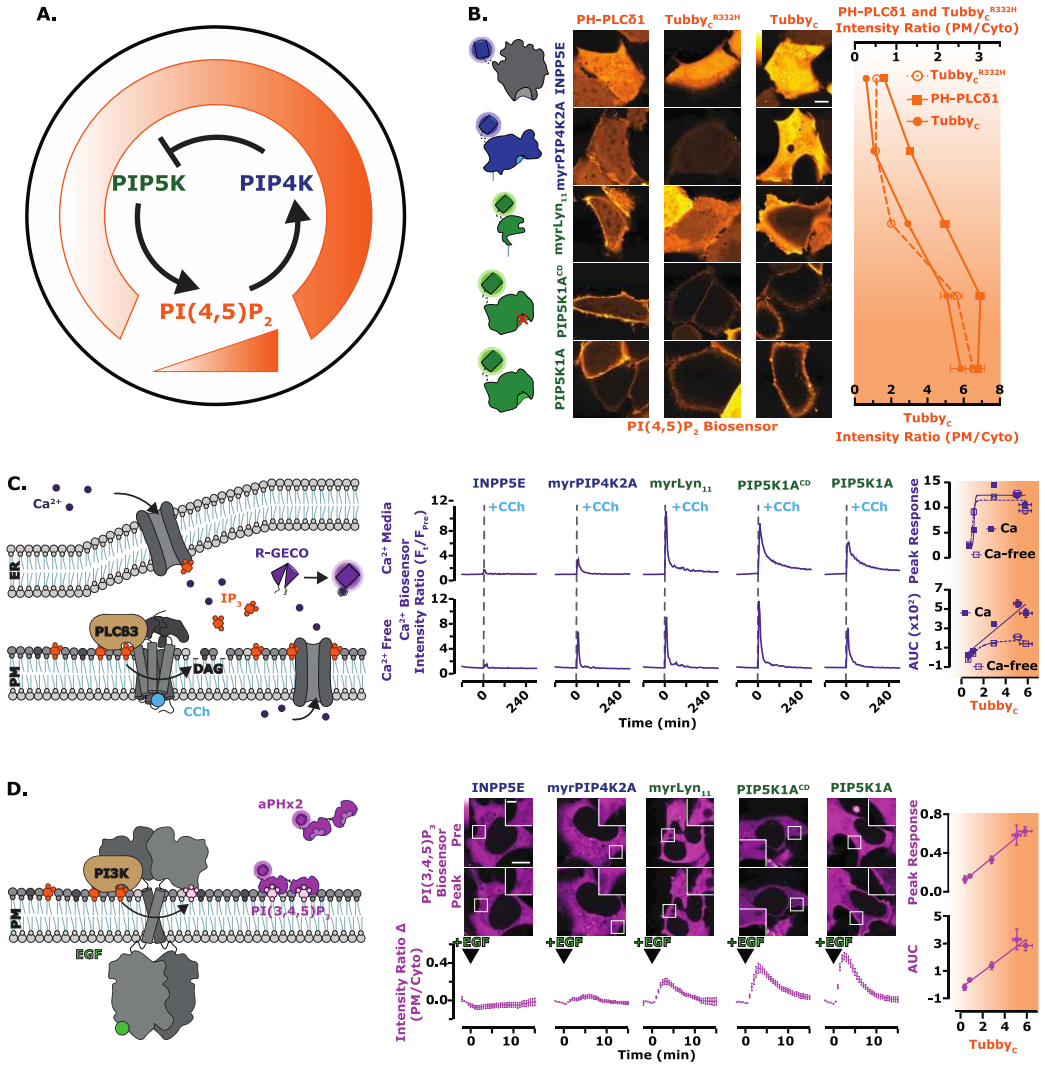

Fig. 4. PI3K, but not calcium signaling, are modulated across all concentration ranges of PI(4,5)P$_2$. (**A**) Proposed regulation of PIP5K by the low affinity PI(4,5)P_2 interaction of PIP4K. The working model for negative feedback of PIP5K via PIP4K resembles the thermostat regulation of temperature. When PI(4,5)P_2 levels are high, PIP4K is recruited and held at the PM, via a direct low affinity interaction with PI(4,5)P_2. At the PM, PIP4K interacts with and inhibits the catalytic activity of PIP5K, causing reduced PI(4,5)P_2 synthesis. (**B**) PI(4,5)P_2 biosensors detect a gradient of lipid levels. HEK293Aå cells were transfected with the indicated fluorescently tagged PI(4,5)P_2 modulating proteins (INPP5E, myrPIP4K2A, myrLyn$_{11}$, PIP5K1A catalytic dead or active) and the indicated PI(4,5)P_2 biosensor (PH-PLCδ1, Tubby, or Tubby^{R332H} displayed in orange) for 16-24 hours. Mean fluorescence intensity (PM/cyto) are shown as points with error bars representing s.e. of >120 cells imaged across three independent experiments. (**C**) PLC-mediated Ca^{2+} signals saturate at tonic PI(4,5)P_2 levels. Cartoon schematics of PLC mediated Ca^{2+} signaling and detection. HEK293A cells were transfected with the indicated fluorescently tagged construct and the calcium sensor R-GECO (purple). During time-lapse confocal microscopy (performed with either compete imaging media containing 1.8 mM Ca^{2+} [Ca^{2+}] or calcium free Ringer's media [Ca^{2+}-Free]), cells were stimulated with 100 µM CCh as indicated. Traces represent the peak response of mean change in fluorescence intensity (F_t/F_{Pre} normalized to pre-stimulation levels) ± s.e. of >100 cells imaged across a minimum of three independent experiments. The peak response and total area under the curve (AUC) were plotted against the normalized ratio of Tubby$_C$. (**D**) PI3K mediated PI(3,4,5)P_3 synthesis is linearly dependent on PI(4,5)P_2 levels. Cartoon schematics show PI3K mediated signaling and detection of PI(3,4,5)P_3 upon the addition of EGF. HEK293A cells were transfected with the indicated fluorescently tagged construct and the PI(3,4,5)P_3 biosensor, PH-ARNO$^{2G\text{-}I303Ex2}$ (aPHx2) (magenta). During time-lapse confocal microscopy, cells were stimulated with 10 ng/mL EGF, as indicated. Traces represent the peak response of mean change in fluorescence intensity (change in PM/cell from pre-stimulation levels) ± s.e. of 35 cells imaged across a minimum of three independent experiments. The peak response and AUC were plotted against the normalized ratio of Tubby$_C$.